

OPTIMAL ZEM-BASED MIDCOURSE GUIDANCE FOR INTERCEPTORS USING TRAJECTORY PREDICTION

Sumin Kim[1], Ki-Wook Jung[1] & Chang-Hun Lee[1]

[1]Korea Advanced Institute of Science and Technology(KAIST), Daejeon 34141, Republic of Korea

Abstract

This paper proposes a quasi-optimal midcourse guidance law for anti-ballistic missiles, offering a practical balance between optimality and real-time feasibility under complex aerodynamic and thrust profiles. The guidance command is derived from an explicit relationship between lateral acceleration and flight path angle dynamics, guaranteeing finite-time Zero-Effort-Miss (ZEM) convergence. To achieve computational efficiency, stage-specific assumptions are utilized to derive a simplified quasi-optimal guidance command, significantly reducing computational load while maintaining negligible deviation from the true optimal solution. Numerical simulations, including comparisons with optimal trajectories obtained through direct trajectory optimization, demonstrate the near-optimality of the proposed guidance law. Furthermore, Monte Carlo simulations confirm strong robustness against modeling uncertainties. The proposed guidance law also maintains high interception accuracy and computational efficiency suitable for real-time implementation.

Keywords: Missile Interception, Zero-Effort-Miss, Ballistic Trajectory Prediction, Optimal Midcourse Guidance

1. Introduction

The rapid proliferation of ballistic missile threats has underscored the critical importance of high-altitude interception systems. These systems should function effectively across both atmospheric and exo-atmospheric flight regimes. During the atmospheric flight phase, the guidance strategy should focus on minimizing aerodynamic control effort to maintain the interceptor's kinetic performance and stability. However, as the vehicle ascends to high altitudes where the thin atmosphere renders conventional aerodynamic fin control ineffective, the system should transition to using lateral thrusters, such as the Divert and Attitude Control System (DACS). Unlike aerodynamic control, the DACS operates on strictly limited propellant, which requires minimizing propellant consumption rather than merely minimizing a quadratic control-energy metric—to secure sufficient maneuverability for the subsequent terminal phase. Consequently, operating within complex flight dynamics governed by the continuous interplay of thrust, varying aerodynamic forces, and gravity, high-altitude interceptors should concurrently satisfy these composite requirements to ensure a successful engagement.

Extensive research has been dedicated to developing effective midcourse guidance laws. To ensure computational speed, previous research on midcourse guidance has relied on closed-form solutions, such as Keplerian methods [1]. These analytical approaches allow for rapid trajectory prediction, facilitating the calculation of the required velocity for Lambert guidance applications [2]. However, a critical drawback of these methods is that they inherently neglect aerodynamic forces. In realistic interception scenarios, this simplification leads to accumulated prediction errors. Consequently, misinterpreting aerodynamic deceleration as a trajectory deviation triggers unnecessary corrective maneuvers, leading to inefficient fuel consumption and resource depletion. Beyond the issue of modeling accuracy, existing predictive guidance laws have primarily focused on satisfying terminal kinematic constraints without explicitly formulating an energy-optimal problem [3]. This limitation is

particularly critical for interceptors equipped with DACS, where failing to minimize control effort can rapidly deplete the finite fuel reserves. To account for aerodynamic effects, high-fidelity approaches using Response Surface Models (RSM) [4] have been explored. Despite their improved accuracy, these methods suffer from critical practical limitations. RSM incurs prohibitive offline computational costs and lacks flexibility in adapting to mission changes. Additionally, its reliance on interpolation may introduce approximation errors that can degrade guidance performance.

To overcome these limitations, this study proposes a quasi-optimal midcourse guidance law. We formulate the guidance problem as a finite-time tracking problem that explicitly minimizes the control energy performance index. In this framework, we derive an explicit expression for the control effectiveness of lateral acceleration on the flight path angle (FPA) and apply finite-time convergence error dynamics to ensure the Zero-Effort-Miss (ZEM) converges to zero. The proposed law is specifically designed to reduce guidance errors during the boost phase, thereby minimizing the cumulative control demand on the DACS and preserving its finite fuel for the subsequent terminal phase. Phase-specific assumptions tailored for the entire engagement—spanning the boost, coast, and kill vehicle (KV) phases—are also introduced to achieve highly efficient computational performance. Finally, comprehensive numerical simulations are conducted to thoroughly validate the performance and practical feasibility of the proposed guidance law. First, the validity of the phase-specific assumptions is directly confirmed by analyzing the trajectory data extracted from the numerical simulations. Subsequently, the near-optimality of the derived command is assessed through a comparative analysis with the true optimal trajectories generated by the GPOPS-II optimization software [5]. Furthermore, Monte Carlo simulations demonstrate the robustness of the proposed method against various modeling uncertainties, such as thrust variations and aerodynamic dispersions. Ultimately, the results confirm that the proposed midcourse guidance law successfully minimizes control energy and maintains high interception accuracy while remaining suitable for real-time onboard implementation.

The remainder of this paper is organized as follows. Section 2 presents the problem formulation, detailing the dynamic model and the trajectory prediction method. Section 3 derives the optimal ZEM-based guidance law. This section establishes the optimal error dynamics and the optimal guidance command, followed by the development of phase-specific quasi-optimal guidance laws tailored for the boost, coast, and KV phases. Section 4 provides comprehensive numerical simulations, outlining the simulation conditions and evaluating the numerical results across all flight phases. Furthermore, this section evaluates the near-optimality of the proposed method through comparative analysis and analyzes its robustness under modeling uncertainties. Finally, Section 5 summarizes the concluding remarks.

2. Problem Formulation

The overall engagement scenario considered in this study is systematically divided into two sequential phases: the interceptor phase and the KV phase. The interceptor phase is further categorized into a boost phase and a subsequent coast phase. Specifically, the coast phase progresses within the atmospheric layer where sufficient control authority can be secured via aerodynamic forces until the vehicle reaches a transition altitude of 40 km. Upon exceeding this 40 km altitude threshold, the main booster is separated, and the system transitions to the exoatmospheric KV phase. During the KV phase, because aerodynamic forces vanish due to the extremely low air density, a Divert Control System (DCS) is utilized to directly generate normal acceleration for maneuverability.

Furthermore, two main assumptions are used. First, for the short flight duration considered, the planar coordinate system is treated as an inertial frame. Second, the location of the predicted intercept point (PIP) is assumed to be known a priori.

2.1 Interceptor Model

The interceptor is modeled as a point mass in a 2D plane, as illustrated in Fig. 1. The dynamics of the interceptor are described as follows:

$$\dot{x} = V\cos\gamma, \quad \dot{y} = V\sin\gamma, \quad \dot{V} = \frac{T\cos\alpha - F_D(\alpha)}{m} - g(y)\sin\gamma$$
$$\dot{\gamma} = \frac{T\sin\alpha + F_L(\alpha) - mg(y)\cos\gamma}{mV}, \quad \dot{m} = -\frac{T}{gI_{sp}}\,(t \le t_{BO}) \tag{1}$$

x and y represent the position (range and altitude) of the interceptor, while V and m denote its speed and mass. The parameter I_{sp} is the specific impulse, and T, F_D, and F_L correspond to the thrust, drag, and lift forces, respectively. The trajectory comprises a boost phase ($t \le t_{BO}$, variable mass) and a coast phase ($t > t_{BO}$, constant mass).

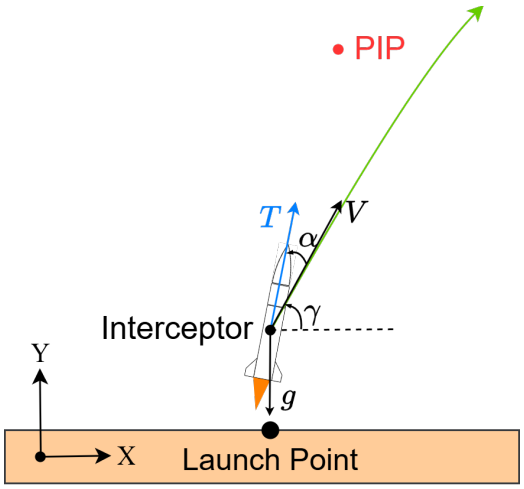


Figure 1 – Dynamics of interceptor

2.2 Kill Vehicle Model

The equations of motion for the KV are fundamentally identical to those of the interceptor. However, since the KV operates at exoatmospheric altitudes characterized by extremely low air density, aerodynamic forces are negligible and thus omitted from the dynamic model. Furthermore, for attitude and trajectory control, the KV utilizes a DCS rather than aerodynamic fins, directly generating normal acceleration to maneuver. The engagement geometry and the forces acting on the KV are illustrated in Fig. 2.

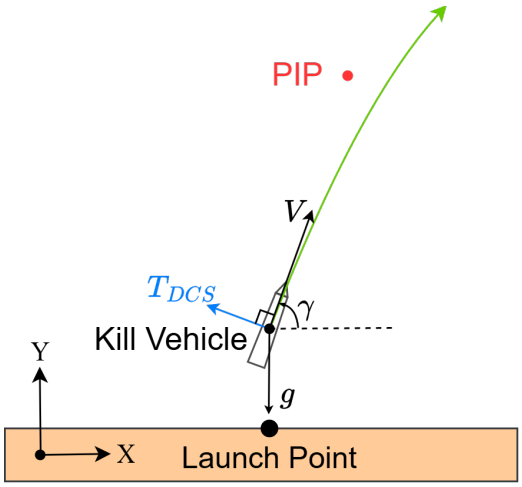


Figure 2 – Dynamics of kill vehicle

The dynamics of the KV are described as follows:

$$\dot{x} = V\cos\gamma, \quad \dot{y} = V\sin\gamma, \quad \dot{V} = -g(y)\sin\gamma, \quad \dot{\gamma} = \frac{T_{DCS} - mg(y)\cos\gamma}{mV}, \quad \dot{m} = -\frac{T_{DCS}}{gI_{sp,DCS}} \tag{2}$$

In Eq.(2), the state variables for position (x, y), speed (V), and mass (m) are defined identically to those of the interceptor. $I_{sp,DCS}$ represents the specific impulse of the DCS, and T_{DCS} corresponds to the lateral thrust. Unlike the preceding coast phase, the KV mass becomes variable again due to DCS fuel consumption.

2.3 Trajectory Prediction Method

For the coast phase trajectory estimation, the PCS(Partial Closed-form Solution) is formulated based on the closed-form analytical solution [6] obtained by considering the motion in a scenario where the drag coefficient remains constant. The closed solution of the scenario is as follows:

$$V(\gamma) = \frac{V_0 \cos\gamma_0}{\cos\gamma\sqrt{1+\beta V_0^2 \cos^2\gamma_0(\phi(\gamma_0)-\phi(\gamma))}}$$
$$\text{where } \phi(\gamma) \triangleq \frac{\sin\gamma}{\cos^2\gamma} + \ln\left[\tan\left(\frac{\gamma}{2}+\frac{\pi}{4}\right)\right],\ \beta = \frac{\rho S_{ref} C_D}{2mg} \tag{3}$$

For the boost phase, the trajectory is predicted using the 4th-order Runge-Kutta method(RK4), while the coast phase is discretized into PCS segments at regular γ intervals [7].

$$t_{k+1} = t_k + \frac{2[V_k \sin\gamma_k - V_{k+1}\sin\gamma_{k+1}]}{g_k(2+\mu_k)},\quad x_{k+1} = x_k + \frac{V_k^2 \sin 2\gamma_k - V_{k+1}^2 \sin 2\gamma_{k+1}}{2g_k(1+\mu_k)}$$
$$y_{k+1} = y_k + \frac{V_k^2 \sin^2\gamma_k - V_{k+1}^2 \sin^2\gamma_{k+1}}{g_k(2+\mu_k)},\quad \text{where } \mu_k \triangleq \beta_k(V_k^2 \sin\gamma_k + V_{k+1}^2 \sin\gamma_{k+1}) \tag{4}$$

3. Optimal ZEM-based Guidance Law

3.1 Optimal Error Dynamics

To ensure the finite-time convergence of the ZEM, we adopt the finite-time optimal error dynamics proposed in [8]. The tracking formulation for the missile guidance problem is expressed as:

$$\dot{\varepsilon}(t) = g(t)u(t) \tag{5}$$

where $\varepsilon(t)$ is the tracking error, $g(t)$ represents the time-varying control efficiency, and $u(t)$ denotes the control input. In this framework, the tracking error $\varepsilon(t)$ is equivalent to the ZEM (Z), the geometric definition of which is illustrated in Fig. 3.

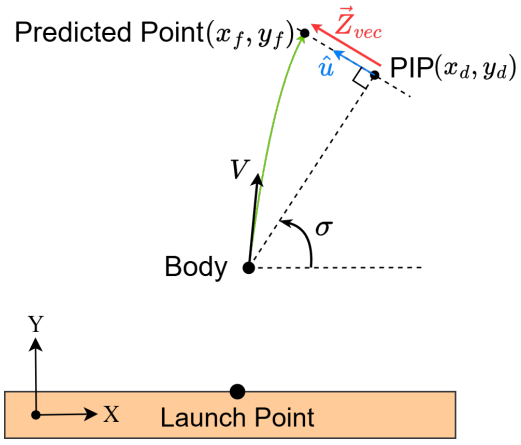


Figure 3 – Definition of ZEM

As illustrated in Fig. 3, the predicted point is defined as the intersection of the Line-of-Sight (LOS) frame and the interceptor's predicted trajectory. This point is determined by numerically propagating the trajectory through integration, where the intersection is efficiently found using the Secant method. The distance vector $\vec{Z}_{vec}$ is then expressed as:

$$\vec{Z}_{vec} = [x_f - x_d, y_f - y_d]^T \tag{6}$$

Subsequently, the ZEM is defined by projecting this distance vector onto the axis normal to the LOS:

$$Z = \vec{Z}_{vec} \cdot \hat{u} \quad \text{where} \quad \hat{u} = [-\sin\sigma, \cos\sigma]^T \tag{7}$$

The unit vector $\hat{u}$ is defined as the normal to the LOS. By differentiating the ZEM with respect to time, the relationship between the tracking model and the missile kinematics is established as follows:

$$\begin{aligned} \dot{\varepsilon}(t) = \dot{Z} = \frac{\partial Z}{\partial \gamma}\frac{d\gamma}{dt} = \frac{\partial Z}{\partial \gamma}\frac{1}{V}a_n \\ g(t) = \frac{\partial Z}{\partial \gamma}\frac{1}{V}, \quad u(t) = a_n \end{aligned} \tag{8}$$

In Eq.(8), the term $d\gamma/dt$ represents the FPA rate specifically induced by the control command. Since the ZEM is computed by integrating the full nonlinear equations of motion including gravitational effects, the resulting control efficiency $g(t)$ purely reflects the sensitivity of the error to the control input. Notably, because gravitational acceleration is already embedded in the predicted "zero-effort" trajectory, it does not contribute to the partial derivative of the ZEM rate with respect to the control. Consequently, by substituting $d\gamma/dt = a_n/V$, the mapping $\dot{\varepsilon} = g(t)u$ serves as a valid linear-like sensitivity model. To further enhance fidelity, the sensitivity term $\partial Z/\partial\gamma$ is evaluated via numerical differentiation, thereby capturing the nonlinear relationship between the FPA and the ZEM more accurately.

Following [8], the finite-time optimal error dynamics are governed by:

$$\dot{\varepsilon}(t) + \frac{\Gamma(t)}{t_{go}}\varepsilon(t) = 0, \quad \text{where } \Gamma(t) = \frac{t_{go}R^{-1}(t)g^2(t)}{\int_t^{t_f} R^{-1}(\tau)g^2(\tau)\,d\tau} \tag{9}$$

This dynamics implies that the control input minimizes the following cost function:

$$J = \int_t^{t_f} R(\tau)u^2(\tau)\,d\tau, \quad \text{with } R(\tau) = \frac{1}{t_{go}^{k_{gid}-1}} \tag{10}$$

where $R(\tau)$ is the weighting function, t_f is the intercept time, and k_{gid} is the guidance gain.

3.2 Optimal Guidance Law for Interceptor

Substituting Eq.(8) into Eq.(9) yields the guidance command $a_n(t)$ as follows:

$$a_n(t) = -\frac{V}{\partial Z/\partial\gamma}\frac{\Gamma(t)}{t_{go}}Z, \quad \text{with } \Gamma(t) = \frac{(\partial Z/\partial\gamma)^2 t_{go}^{k_{gid}}/V^2}{\int_t^{t_f}(\partial Z/\partial\gamma)^2 t_{go}^{k_{gid}-1}/V^2\,d\tau} \tag{11}$$

While theoretically precise, this proposed guidance law poses practical challenges for direct evaluation due to two major computational burdens. First, evaluating the integral term in $\Gamma(t)$ requires the numerical computation of the sensitivity term $(\partial Z/\partial\gamma)$ continuously from the current time t to the predicted intercept time t_f. Second, because the exact value of t_f is determined only after the full trajectory prediction is completed, the integral cannot be evaluated concurrently with the prediction step. Consequently, the guidance processor should store the entire sequence of the predicted state variables to calculate the integral retroactively, leading to a substantial memory footprint. To overcome these implementation challenges, the following subsection proposes a computationally efficient quasi-optimal guidance law. By adopting appropriate physical assumptions for each flight phase—specifically the boost and coast phases—the complex integral and sensitivity analysis are simplified into a practically feasible form.

3.3 Quasi-Optimal Guidance Law for Interceptor

Boost Phase In the boost phase, the speed of the interceptor (V) changes much faster than the sensitivity term $\partial Z/\partial\gamma$. Based on this, we assume $\partial Z/\partial\gamma$ is constant during this interval to simplify the derivation. Also, the time-to-go (t_{go}) is defined as the remaining boost time ($t_{go} = t_{BO} - t$). Then, the guidance law for the boost phase is given by:

$$a_n(t) = -\frac{V}{\partial Z/\partial\gamma}\frac{\Gamma(t)}{t_{go}}Z, \quad \text{with } \Gamma(t) = \frac{t_{go}^{k_{gid}}/V^2}{\int_t^{t_f} t_{go}^{k_{gid}-1}/V^2\, d\tau} \tag{12}$$

The choice of t_{go} not only allows the integral term to be calculated simultaneously during the trajectory prediction, but also forces the guidance law to eliminate most of the tracking errors within the boost phase. As a result, it minimizes the residual errors that the DACS should correct in the subsequent phases.

Coast Phase In the coast phase, the sensitivity term $\partial Z/\partial\gamma$ becomes dominant. Unlike the boost phase, this sensitivity term cannot be treated as a constant, so we employ a different error dynamics formulation for this phase. After the boost phase, the interceptor reaches a high altitude and high speed. Due to the thin atmosphere and high velocity, both aerodynamic drag and gravitational effects can be neglected. These assumptions are introduced solely for deriving the analytical guidance law and are not used in the actual trajectory prediction process. Under these assumptions, the engagement geometry is illustrated in Fig. 4:

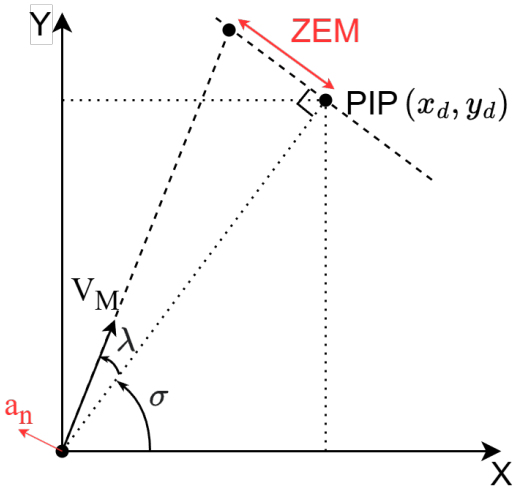


Figure 4 – Engagement geometry of coast phase

This engagement geometry is identical to that of Proportional Navigation (PN). Under the small-angle and constant-speed assumptions, the ZEM and its time derivative can be derived as Eq.(13).

$$\begin{aligned} Z &= y + vt_{go} \\ \dot{Z} &= -t_{go}a_\sigma \end{aligned} \tag{13}$$

where y and v represent the relative position and velocity perpendicular to the LOS, respectively, and a_σ denotes the acceleration command normal to the LOS. Additionally, the heading angle λ is defined as the error angle between the LOS direction and the velocity vector, which represents the heading misalignment that induces the ZEM. Since most of the ZEM is already eliminated during the preceding boost phase, the heading angle λ remains very small throughout the coast phase. Under this small-angle condition ($\lambda \approx 0$), the acceleration command normal to the LOS (a_σ) can be closely approximated as the interceptor's normal acceleration command (a_n). As a result, the error dynamics can be expressed as:

$$\begin{aligned} \dot{\varepsilon}(t) &= \dot{Z} = -t_{go}a_n \\ g(t) &= -t_{go}, \quad u(t) = a_n \end{aligned} \tag{14}$$

Following [8], the finite-time optimal error dynamics are governed by:

$$\dot{\varepsilon}(t)+\frac{\Gamma(t)}{t_{go}}\varepsilon(t)=0, \quad \text{where } \Gamma(t)=k_{gid}+2 \tag{15}$$

Finally, the acceleration command is derived as:

$$a_n=\frac{k_{gid}+2}{t_{go}^2}Z \tag{16}$$

Although this guidance command is mathematically derived under simplified and approximated engagement geometry, the actual implementation utilizes the unapproximated, full-fidelity predicted trajectory to evaluate the ZEM. By directly injecting the non-approximated trajectory prediction into the guidance loop, the geometric linearization errors inherent in conventional analytical laws are significantly eliminated.
Consequently, the mathematical form of this coast phase acceleration command is identical to that of conventional PN. However, the proposed command achieves superior interception performance compared to standard PN because the ZEM is evaluated using full numerical trajectory prediction rather than simple linearized geometric approximations, thereby capturing the true intercept error more precisely.

3.4 Optimal Guidance Law for Kill Vehicle

When the available aerodynamic force for control decreases during the coast phase, the booster is separated, leaving only the KV. In this phase, the KV directly generates the required normal acceleration using its DACS. Unlike the previous two phases where the aerodynamic force is available, the guidance law for this phase minimizes the 1-norm of the acceleration. This formulation is adopted to conserve the remaining fuel, thereby maximizing the control margin available for the subsequent terminal phase.
Since this phase also features low air density and high interceptor speed, the engagement geometry and its corresponding error dynamics remain identical to those of the coast phase illustrated in Fig. 4. To derive the fuel-optimal guidance law, the optimization problem is formulated using Pontryagin's Minimum Principle (PMP). The performance index to be minimized and its constraints are defined as:

$$J=\int_t^{t_f}|a_n(\tau)|d\tau \quad \text{s.t.} \begin{cases} \dot{Z}=-t_{go}a_n \\ Z(t_f)=0 \\ -a_{max}\le a_n\le a_{max} \end{cases} \tag{17}$$

To apply PMP, the Hamiltonian H is constructed by combining the running cost and the system dynamics with a costate $\lambda(\tau)$:

$$H=|a_n(\tau)|-\lambda(\tau)t_{go}a_n(\tau) \tag{18}$$

According to the costate equation, the time derivative of $\lambda(\tau)$ is governed by:

$$\dot{\lambda}(\tau)=-\frac{\partial H}{\partial Z}=0 \tag{19}$$

Eq.(19) implies that the costate is a constant over the remaining flight time, i.e., $\lambda(\tau)=\lambda_f$. The sign of λ_f is determined such that the terminal constraint $Z(t_f)=0$ is satisfied. To minimize the Hamiltonian with respect to the control input $a_n(\tau)$, the optimality condition requires:

$$a_n^*(\tau)=\arg\min_{a_n}\left[|a_n(\tau)|-\lambda_f(t_f-\tau)a_n(\tau)\right] \tag{20}$$

Due to the non-differentiable nature of the 1-norm term $|a_n|$, the optimal control law that minimizes Eq.(20) is directly derived in a bang-off form as follows:

$$a_n^*(\tau)=\begin{cases} a_{max}\text{sgn}(\lambda_f) & \text{if } |\lambda_f|t_{go}>1 \\ 0 & \text{if } |\lambda_f|t_{go}\le 1 \end{cases} \tag{21}$$

Eq. (21) indicates that since λ_f is a constant and t_{go} monotonically decreases, the optimal control naturally exhibits a bang-off structure. This control profile applies maximum acceleration during the initial phase to aggressively eliminate the ZEM, followed by a coasting phase where the command drops to zero. Although this optimal behavior could theoretically be replicated by directly feeding back the predicted ZEM (Z), practical implementations face significant challenges. In the presence of modeling uncertainties, navigation errors, and dynamic variations in the PIP, the numerically evaluated ZEM never remains perfectly at zero. Continuously enforcing zero-error regulation against these residual fluctuations induces severe high-frequency chattering in the acceleration command. To resolve this practical issue and prevent excessive control actuation while maintaining the ZEM within a small neighborhood of zero, a dead-zone threshold denoted as a design parameter δ is introduced. Consequently, the final optimal feedback guidance command is constructed as follows:

$$a_n = \begin{cases} -a_{max} \cdot \mathrm{sgn}(Z) & \text{if } |Z| \geq \delta \\ 0 & \text{if } |Z| < \delta \end{cases} \tag{22}$$

where δ represents a dead-zone threshold. In practical or numerical environments, the predicted ZEM ($|Z|$) can never be exactly zero due to numerical truncation errors and discretization limits. Without a dead-zone, even minor numerical fluctuations would trigger indiscriminate or excessive thruster firings, quickly depleting the fuel. Therefore, by introducing δ, the guidance law prevents such unnecessary commands and applies maximum thrust only when the predicted miss distance exceeds this tolerable numerical limit.

4. Numerical Simulation

4.1 Simulation Condition

To enhance engineering realism and reflect practical implementation constraints, a multi-rate simulation framework is utilized where the guidance loop operates at a discrete sampling frequency of 100 Hz. All numerical simulations are performed using MATLAB 2024b on a desktop computer equipped with an Intel Core i7-14700K CPU. The gravitational acceleration $g(y)$ is implemented using the inverse-square law to precisely account for the significant altitude variations during the exoatmospheric flight, defined as:

$$g(y) = \frac{GM_e}{(R_e + y)^2} \tag{23}$$

where G is the universal gravitational constant, M_e is the mass of the Earth, and R_e is the mean radius of the Earth.

Interceptor In the Boost and Coast Phase simulations, the commanded angle of attack (AoA), denoted as α_c, is utilized as the control input and is computed as follows:

$$\alpha_c = \frac{ma_{n,c}}{T + C_{L,\alpha}\bar{q}S_{ref}} \tag{24}$$

where m is the mass of the interceptor, $a_{n,c}$ is the commanded normal acceleration, T is the thrust, $C_{L,\alpha}$ denotes the lift coefficient slope linearized with respect to the AoA, $\bar{q}$ represents the dynamic pressure, and S_{ref} is the reference aerodynamic area.
The specific simulation parameters and initial states for the Interceptor phase are summarized in Table 1. The aerodynamic lift and drag coefficients are determined via multi-dimensional interpolation of a look-up table based on the Mach number and AoA. Additionally, the maximum allowable AoA is strictly constrained to 10° to maintain aerodynamic stability.

Kill Vehicle For the KV phase, the specific simulation parameters and initial states are summarized in Table 2. Unlike the preceding phases that rely on aerodynamic control surfaces, the guidance command in this stage is executed via direct thrust from the DACS to generate the required normal acceleration. Furthermore, since the KV operates at an altitude where the atmospheric density is extremely sparse, all aerodynamic forces are treated as negligible.

Table 1 – Simulation parameters and initial conditions for the interceptor phase

Parameters	Value	Unit
Predicted Intercept Point, (PIP_x, PIP_y)	(40.0, 100.0)	km
Rocket motor burn time, t_{BO}	11.955	sec
Initial position, (x_0, y_0)	(0.0, 0.0)	km
Initial velocity, V_0	100.0	m/s
Initial flight path angle, γ_0	85.0	deg
Maximum allowable AoA, α_{max}	10.0	deg

Table 2 – Simulation parameters and initial conditions for the kill vehicle phase

Parameters	Value	Unit
Predicted Intercept Point, (PIP_x, PIP_y)	(40.0, 100.0)	km
Initial position, (x_0, y_0)	(10.0, 40.0)	km
Initial velocity, V_0	2000.0	m/s
Initial flight path angle, γ_0	80.0	deg
ZEM convergence threshold, δ	10.0	m
Maximum Thrust of DCS, $T_{max,DCS}$	3000	N

4.2 Numerical Results of Interceptor

A parametric study is performed by varying the guidance gain ($k_{gid} = 1, 2, 3$) to investigate its impact on guidance performance. The resulting trajectories and control profiles are illustrated in Fig. 5.

From the simulation results in Fig. 5, it can be observed that the guidance gain k_{gid} directly governs the time-varying characteristics of the control profiles. As k_{gid} increases, the time-to-go weight in the performance index imposes a progressively heavier penalty on the control input toward the end of the boost phase. To satisfy the terminal constraints under this stringent late-stage restriction, the guidance system is mathematically driven to resolve most of the predicted miss distance as early as possible, causing the acceleration command to converge to zero more rapidly near the terminal time. This mechanism inherently demands a larger guidance command during the initial stage of the flight. Specifically, as shown in Fig. 5, the acceleration command is highly concentrated in the early phase of the flight where the interceptor's velocity is relatively low. Allocating the control effort during this low-speed period allows for more aerodynamic maneuverability and efficient trajectory corrections. This early concentration of control input is clearly reflected in the rapid variations of the flight path angle (FPA) in Fig. 5, which consequently drives the fast initial convergence of the predicted ZEM observed in Fig. 5.

Consequently, the simulation results confirm that all three cases successfully intercept the target, maintaining a final miss distance of less than 0.3 m. Furthermore, the proposed algorithm yields an average computation time of only 0.0923 ms per guidance loop. This remarkably low computational overhead firmly demonstrates the computational efficiency of the proposed algorithm.

Next, the mathematical assumptions introduced in the previous sections are validated using the simulation data, with the verification results presented in Fig. 6. First, the relationship between the sensitivity value ($\partial Z/\partial \gamma$) and the interceptor's speed is investigated during the boost phase. Subsequently, the individual components constituting $g(t)$ in the error dynamics are evaluated and compared to verify the validity of the simplification.

To further justify the simplification of the time-varying gain $\Gamma(t)$ in Eq.(12), the squared scaling factors of the components within the integral are quantitatively evaluated using the boundary values of the boost phase. At the ignition onset ($t = 0$ s), the trajectory sensitivity and velocity are obtained as $\partial Z/\partial \gamma = 162{,}939$ and $V_M = 100$ m/s, respectively. At the end of the boost phase ($t = 11.955$ s), these states transition to $\partial Z/\partial \gamma = 110{,}905$ and $V_M = 2{,}081.02$ m/s.

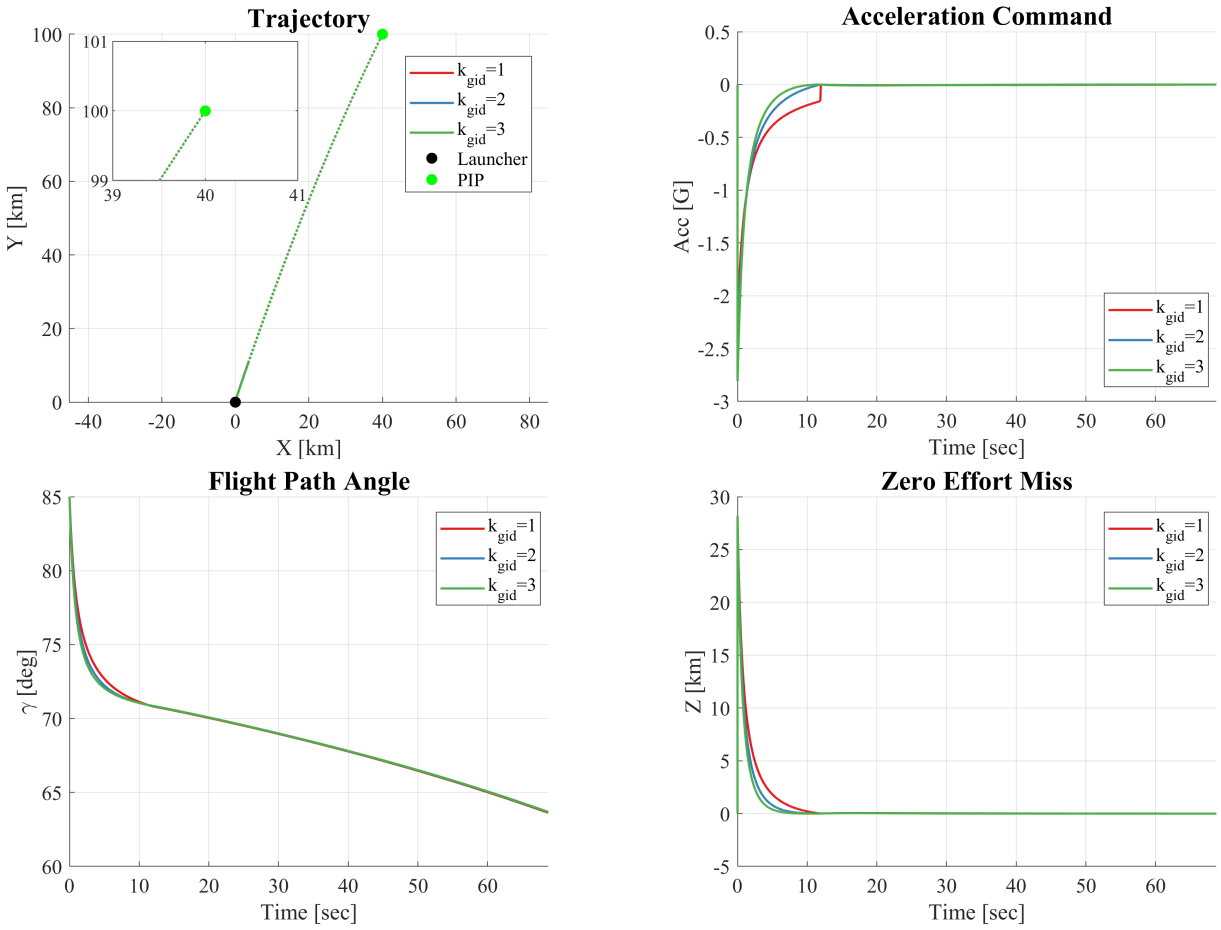
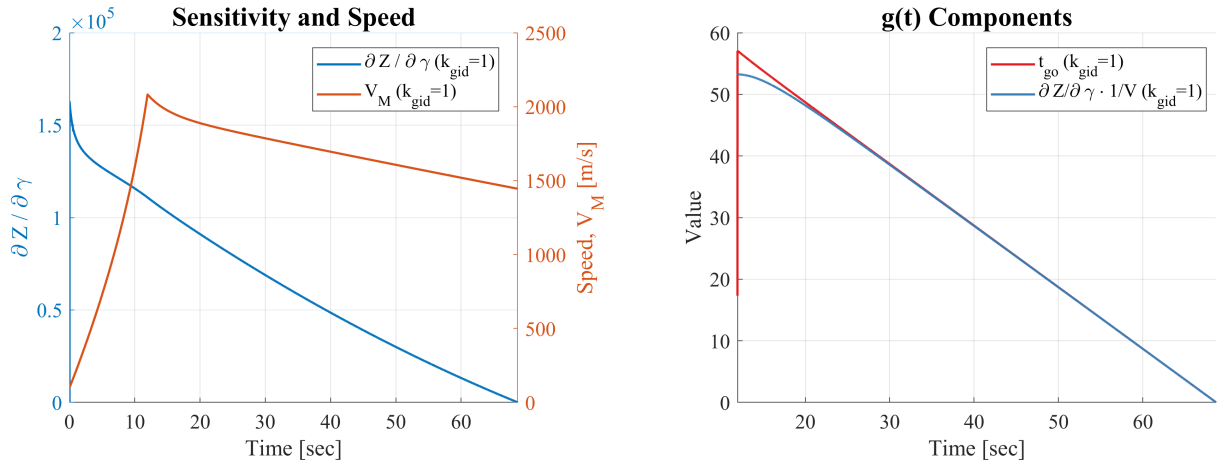


Figure 5 – Simulation results for different guidance gains ($k_{gid} = 1, 2, 3$)



(a) $\partial Z/\partial \gamma$ and Speed

(b) $g(t)$ components

Figure 6 – Verification of the assumptions

By evaluating the ratio of the squared values between the final and initial states, it is revealed that the numerator term $(\partial Z/\partial \gamma)^2$ changes merely by a factor of $110{,}905^2/162{,}939^2 \approx 0.46$ (a 2.17-fold decrease). In stark contrast, the denominator term V^2 escalates significantly by a factor of $2{,}081.02^2/100^2 \approx 433.06$. This overwhelming discrepancy in the squared scaling factors demonstrates that the dynamic variation of the ratio $(\partial Z/\partial \gamma)^2/V^2$ is almost entirely dominated by the acceleration of the vehicle (V^2), whereas the contribution from the trajectory sensitivity variance is practically negligible. Consequently, the sensitivity term $\partial Z/\partial \gamma$ can be reasonably assumed to be a quasi-static constant over the remaining time-of-flight integration interval.

Furthermore, Fig. 6b presents a comparative analysis of the individual components within the control effectiveness function $g(t)$ to verify the approximation model used in the coast phase. Mathematically, the exact formulation of this component is defined as $\frac{\partial Z}{\partial \gamma}\frac{1}{V}$. As observed from the simulation results, a minor discrepancy exists immediately after entering the coast phase (following the rocket motor burnout at $t = 11.955$ s), which is attributed to the presence of residual aerodynamic effects at relatively lower altitudes.
However, after $t = 20$s as the interceptor ascends further, the exact profile and its linear approximation, t_{go}, exhibit good agreement. The two curves overlap almost perfectly throughout the remaining unpowered glide stage until interception. This highly consistent behavior firmly establishes that substituting the complex time-varying states with the simple time-to-go (t_{go}) is a highly accurate and valid simplification for the coast phase.

4.3 Numerical Results of Kill Vehicle

The guidance simulation for the KV is conducted to evaluate the performance and adaptability of the proposed guidance law under the direct thrust control configuration. The resulting flight trajectory, acceleration command, flight path angle, and ZEM profile are illustrated in Fig. 7.

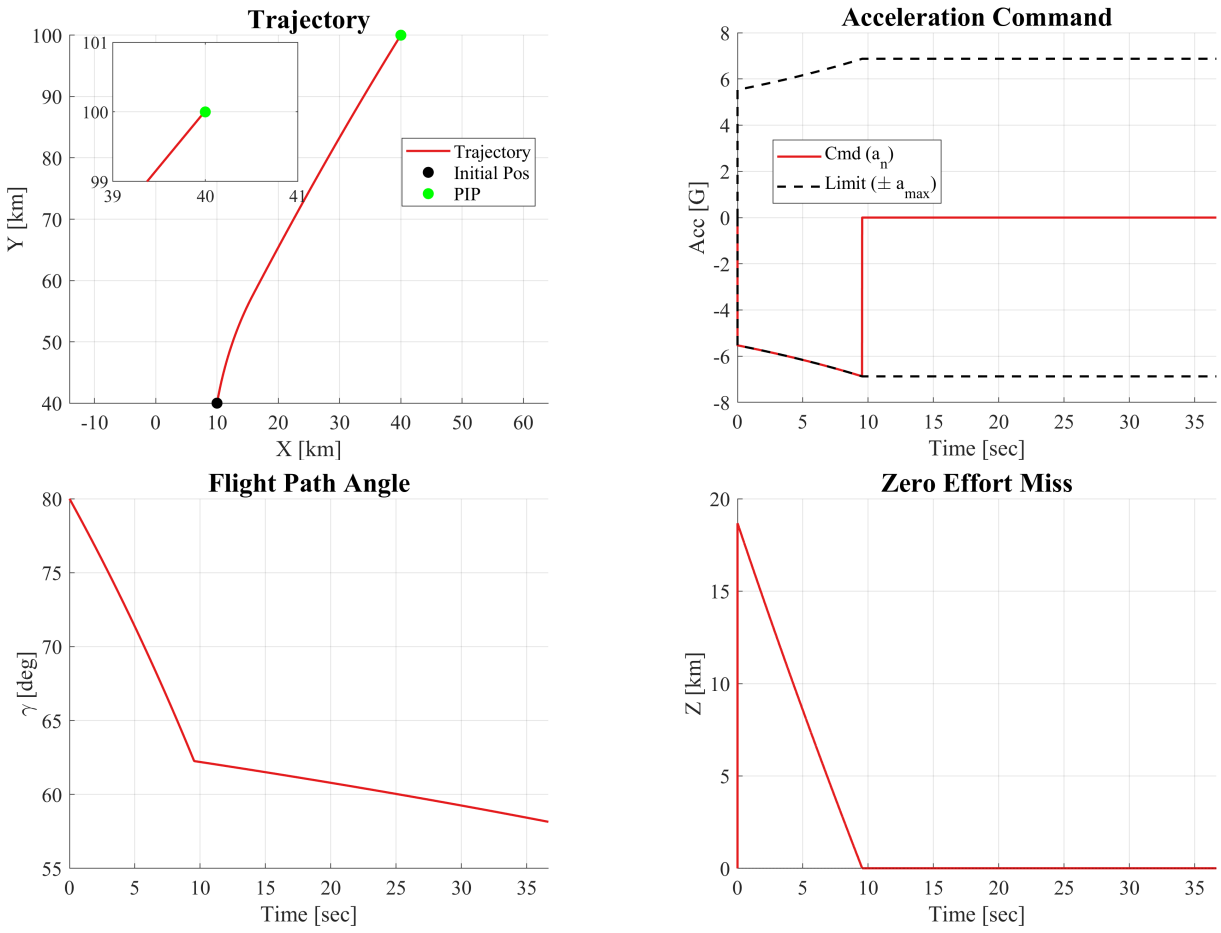


Figure 7 – Simulation results of the Kill Vehicle

As illustrated in the simulation results, the KV successfully intercepts the target, achieving a final miss distance of 7.34 m. Notably, because the guidance law utilizes the accurately predicted ZEM, the resulting control command effectively exhibits the ideal bang-off profile derived from the theoretical optimum. Considering the previously defined convergence boundary ($\delta = 10$ m), this sub-bounding outcome demonstrates the high fidelity and precision of the proposed guidance logic.
Although a tighter convergence boundary could marginally reduce the final miss distance, it inherently induces high-frequency jittering in the guidance commands, which exponentially increases the consumption of unnecessary control energy. Therefore, setting $\delta = 10$ m represents a practical trade-

off that significantly mitigates control jittering and preserves the limited propulsion resource of the DACS. Furthermore, a miss distance of approximately 10 m is a manageable handover error that can be effortlessly eliminated during the subsequent terminal guidance phase, introducing no critical performance degradation.

Additionally, the average computation time is recorded as exceptionally low at 0.0287 ms per guidance loop. This significant reduction in computational overhead compared to the preceding phases is primarily attributed to the simplified guidance architecture tailored for the KV configuration. Because the guidance command in this stage only requires the evaluation of the ZEM profile—completely eliminating the need for multi-dimensional aerodynamic look-up table interpolations or complex trajectory sensitivity matrix computations—the algorithmic complexity is minimized, ensuring a high margin for highly efficient computational performance.

4.4 Optimality Verification of Quasi-Optimal Guidance Law

In this subsection, the optimality of the proposed guidance law is verified by comparison with numerical optimization results obtained using GPOPS-II [5]. Two optimal control scenarios are considered: one allowing continuous acceleration commands throughout the boost and coast phases, representing the absolute theoretical optimum, and another restricting active control to the boost phase only, followed by an uncontrolled coast phase. Since the proposed guidance law is designed to eliminate the predicted ZEM as early as possible during the boost phase, comparison with both scenarios provides insight into how closely the proposed analytical solution approaches the true optimal trajectories under different control execution constraints.

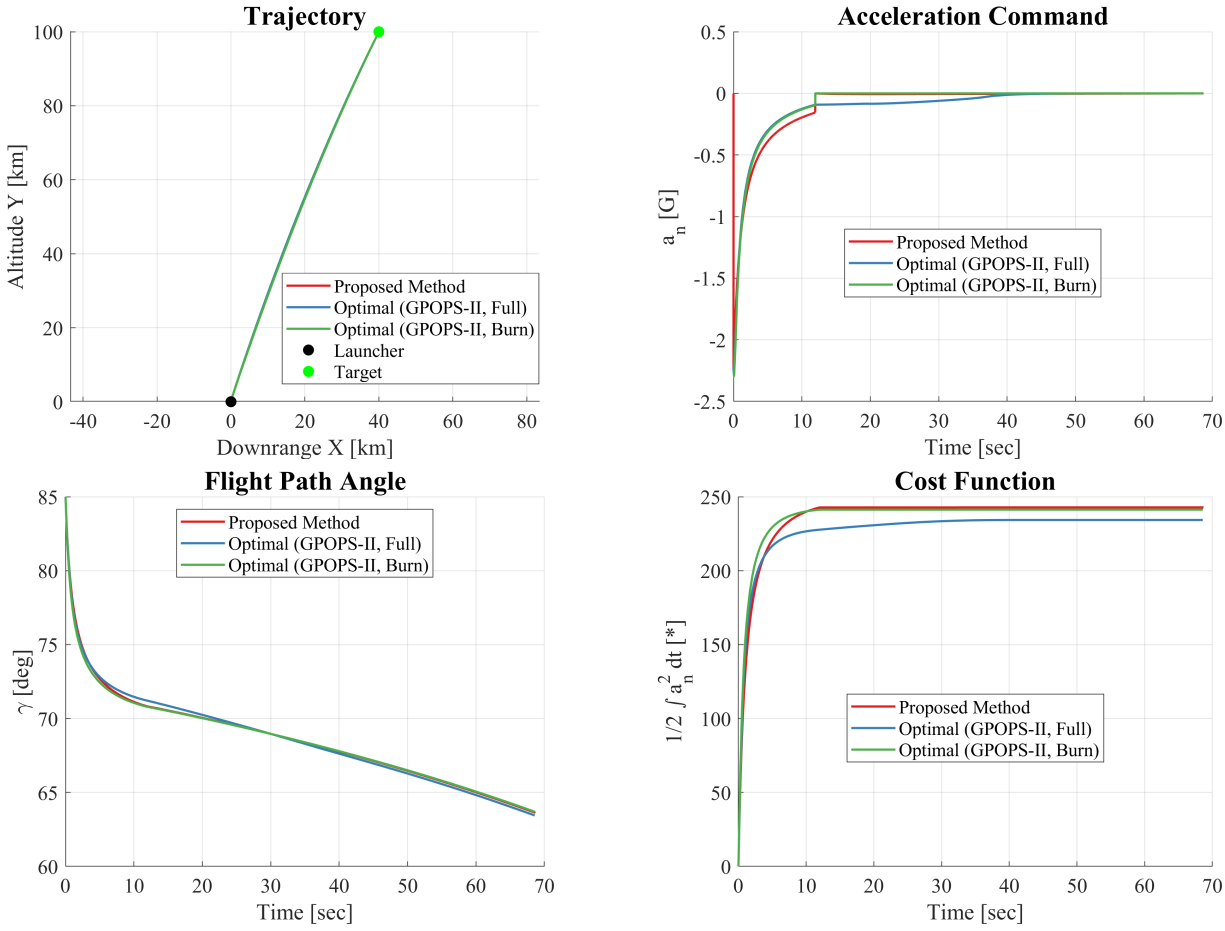


Figure 8 – Optimality verification of the proposed method

The comparison results are illustrated in Fig. 8, and the corresponding quantitative evaluation of the total control costs and optimality errors is summarized in Table 3. The numerical results reveal that the control cost of the proposed method ($J = 242.800$) is remarkably close to that of the boost-phase restricted GPOPS-II solution ($J = 241.279$), yielding an exceptionally low optimality error of only 0.630%.

This minimal discrepancy firmly demonstrates that the proposed analytical guidance law successfully captures the true optimal control behavior under matching physical execution constraints.
Furthermore, when evaluated against the absolute theoretical optimum obtained from the full-interval GPOPS-II scenario ($J = 234.290$), the proposed algorithm still exhibits a highly competitive optimality error of 3.632%. This result implies that the simplified guidance strategy—which mathematically forces the trajectory corrections to be completed within the brief boost phase—introduces a negligible performance penalty while substantially enhancing the computational efficiency. Consequently, the proposed approach is validated as a highly effective and quasi-optimal solution suitable for practical interceptor implementation.

Table 3 – Quantitative comparison of control costs and optimality errors

Case	Control Cost, J	Optimality Error of Proposed Method
Proposed Method (RK4)	242.800	—
GPOPS-II (Full-interval)	234.290	3.632 %
GPOPS-II (Boost-phase)	241.279	0.630 %

4.5 Robustness Analysis under Modeling Uncertainties

In this subsection, the structural robustness and operational reliability of the proposed guidance law are rigorously evaluated by conducting a 500-run Monte Carlo simulation. To faithfully replicate realistic flight environments and capture hardware-induced performance limitations, mathematical perturbations and dynamic actuator delays are systematically incorporated into the nominal system parameters. The nominal parameters and baseline flight states are defined in accordance with the initial conditions previously established in Table 1 and Table 2. Specifically, the initial state variables for the entire simulation engagement—including the launch position, initial velocity, and flight path angle—are primarily governed by the conditions specified in Table 1.
Based on these baseline configurations, aerodynamic uncertainties are modeled by applying standard deviations to both the lift (C_L) and drag (C_D) coefficients. Similarly, thrust uncertainties for both the main booster and the KV propulsion systems are also incorporated. Crucially, the trajectory prediction framework utilizes only the nominal model without incorporating any of these perturbations, ensuring that the guidance law operates under realistic model-mismatch conditions.
Furthermore, the non-ideal response characteristics of the physical control surfaces and the DCS are introduced using first-order system approximations. The dynamic delays are characterized by the respective time constants (τ) for the angle-of-attack (α) response and the DCS thrust generation. These statistical variations and dynamic execution limits ensure a high-fidelity validation environment. The comprehensive set of perturbation parameters and actuator constraints employed for the Monte Carlo analysis is summarized in Table 4.

Table 4 – Perturbation parameters and actuator time constants for Monte Carlo simulations

Parameters	Uncertainty / Value	Unit
Main Booster Thrust Uncertainty, σ_T	10.0	%
KV Propulsion Thrust Uncertainty, $\sigma_{T,KV}$	10.0	%
Drag Coefficient Uncertainty, σ_{C_D}	10.0	%
Lift Coefficient Uncertainty, σ_{C_L}	10.0	%
Actuator Time Constant (α), τ_α	0.25	s
DCS Time Constant, τ_{DCS}	0.01	s

The comprehensive simulation results obtained from the 500-run Monte Carlo analysis, including the dynamic state trajectories, control history, and statistical errors, are presented in Fig. 9. Based on

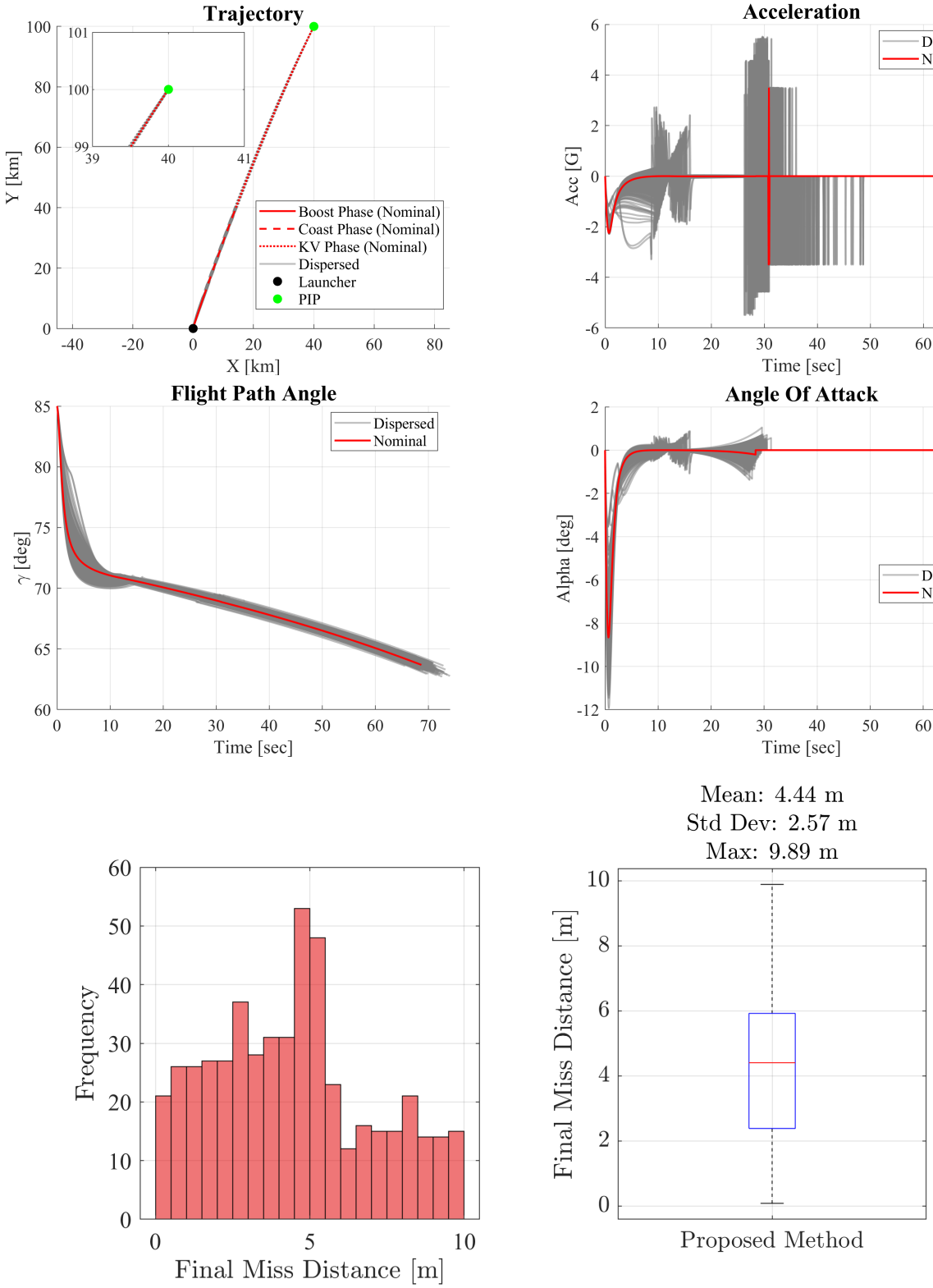


Figure 9 – Optimality and robustness verification results of the proposed method via 500-run Monte Carlo simulations.

these transient responses, the statistical performance is analyzed to evaluate the robustness of the proposed guidance system.

Specifically, Fig. 9 illustrates the final miss distance metrics evaluated at the closest point of approach (CPA) using a quantitative box plot. The numerical analysis yields a mean miss distance of 4.44 m with a standard deviation of 2.57 m.

Crucially, the maximum recorded miss distance across all 500 stochastic samples is bounded at 9.89 m. This worst-case outcome remains strictly within the pre-defined midcourse dead-zone threshold of $\delta = 10$ m, demonstrating that the guidance loop successfully absorbs severe system-level dispersions without triggering any performance degradation or intercept divergence.

This exceptional interception accuracy is mathematically justified by the robust convergence behavior of the guidance command loop. As observed across the flight parameters in Fig. 9, the accumulated errors generated by the combined 10% aerodynamic and thrust uncertainties cause the transient responses to scatter mid-flight. However, the proposed analytical guidance law inherently suppresses these stochastic variations as the interception engagement progresses, forcing all dispersed profiles to stable convergence at the terminal interception point.

Furthermore, even with the presence of non-negligible actuator time delays ($\tau_\alpha = 0.25$ s and $\tau_{DCS} = 0.01$ s), the control commands smoothly guide the missile to eliminate the residual miss distance. The compact distribution within the interquartile range (IQR) of the box plot firmly validates that the proposed ZEM compression scheme delivers highly reliable, repetitive, and robust interception performance under practical operational uncertainties.

5. Conclusion

This study has proposed a quasi-optimal midcourse guidance law formulated as a finite-time tracking problem to minimize control energy while ensuring zero-effort-miss (ZEM) convergence. The numerical results validated the effectiveness of the proposed guidance law through several key findings. First, the guidance command successfully corrected the ZEM profile entirely within the brief rocket motor boost phase, significantly minimizing the cumulative control demand and preserving the finite fuel reserves of the DACS for the subsequent terminal phase. Second, the validity of the phase-specific assumptions introduced to reduce computational complexity was rigorously confirmed. When compared with the optimal trajectories generated by GPOPS-II, the proposed law introduced only a negligible performance penalty while significantly reducing computational burden. Finally, extensive Monte Carlo simulations demonstrated that the final miss distances remained strictly within the prescribed error bounds, indicating strong robustness against critical modeling uncertainties and controller delays. Consequently, the proposed approach provides a highly reliable and computationally efficient framework for advanced multi-phase interception missions.

The Monte Carlo simulations revealed transient acceleration spikes at the end of the boost phase under thrust uncertainties. In practice, these sudden command fluctuations are not expected to significantly affect interception performance, as the physical controller and actuator dynamics cannot track such high-frequency responses. However, this transient behavior remains undesirable for overall guidance stability. Therefore, future research will focus on mitigating these transient command spikes, ensuring smoother command transitions and enhanced robustness against thrust uncertainties.

6. Acknowledgements

This work was supported by Theater Defense Research Center funded by Defense Acquisition Program Administration under Grant UD240002SD.

7. Contact Author Email Address

Sumin Kim: ksm021012@kaist.ac.kr
Ki-Wook Jung: jkw1031@kaist.ac.kr
Chang-hun Lee: lckdgns@kaist.ac.kr

8. Copyright Statement

The authors confirm that they, and/or their company or organization, hold copyright on all of the original material included in this paper. The authors also confirm that they have obtained permission, from the copyright holder of any third party material included in this paper, to publish it as part of their paper. The authors confirm that they give permission, or have obtained permission from the copyright holder of this paper, for the publication and distribution of this paper as part of the ICAS proceedings or as individual off-prints from the proceedings.

References

[1] Dean Zes. Exo-atmospheric intercept with j2 correction. In *Guidance, Navigation, and Control Conference and Exhibit*. American Institute of Aeronautics and Astronautics, 1998.

[2] Shilei Zhao, Wanchun Chen, Liang Yang, and Minghao Wang. Optimal midcourse guidance law for the exo-atmospheric interceptor with solid-propellant booster. *Aerospace Science and Technology*, 127:107670, 2022.

[3] Christian Tournes, Yuri Shtessel, Dimitrios Lianos, David Foreman, and Sreca Jovanov. Interceptor predictive mid-course higher order sliding mode guidance and control. In *AIAA Guidance, Navigation, and Control Conference*. American Institute of Aeronautics and Astronautics, 2009.

[4] Sungjun Ann, Seokwon Lee, Youdan Kim, and Jaemyung Ahn. Midcourse guidance for exoatmospheric interception using response surface based trajectory shaping. *IEEE Transactions on Aerospace and Electronic Systems*, 56(5):3655–3673, 2020.

[5] Michael A. Patterson and Anil V. Rao. Gpops-ii: A matlab software for solving multiple-phase optimal control problems using hp-adaptive gaussian quadrature collocation methods and sparse nonlinear programming. *ACM Trans. Math. Softw.*, 41(1), October 2014.

[6] Peter Chudinov. Approximate analytical description of the projectile motion with a quadratic drag force. *Athens Journal of Sciences*, 1:97–106, 05 2014.

[7] Ki-Wook Jung and Chang-Hun Lee. An impact point guidance for a launch vehicle with aerodynamics control. *IEEE Transactions on Aerospace and Electronic Systems*, 61(5):13565–13579, 2025.

[8] Shaoming He and Chang-Hun Lee. Optimality of error dynamics in missile guidance problems. *Journal of Guidance, Control, and Dynamics*, 41(7):1624–1633, 2018.